Research Article ***http://dx.doi.org/10.4314/mejs.v18i1.6*** ***Open Access***

Evaluations of characteristics of geomagnetic storm (March 23-24, 2023) utilizing several magnetospheric and ionospheric metrics

Gebregiorgis Abraha Fikade[1*], Yikdem Mengesha Gebrehiwot[2] and Yohannes Yirga Kefela[3]

[1]Department of Physics, College of Natural and Computational Sciences, Mekelle University, Ethiopia (*ggabraha@gmail.com; ORCID: https://orcid.org/0009-0004-6478-6636).

[2]Department of Physics, College of Natural and Computational Sciences, Mekelle University, Ethiopia (Yikdem.mengesha@mu.edu.et; ORCID: https://orcid.org/0000-0003-4907-1726).

[3]Department of Mathematics, College of Natural and Computational Sciences, Mekelle University, Ethiopia (yohannes.yirga@mu.edu.et: ORCID: https://orcid.org/0000-0001-8004-8327).

ABSTRACT

This study investigates the ionospheric and geomagnetic response to Coronal Mass Ejection forcing by analyzing Total Electron Content (TEC) distributions, the relationship between the Interplanetary Magnetic Field (IMF) Bz component and the solar-wind convective electric field (Ey), and the temporal evolution of key geospace parameters during disturbed periods. TEC data derived from GNSS-based Global Ionospheric Maps were used to examine spatial variations and storm-time anomalies in ionospheric electron density. Concurrent solar-wind and IMF measurements obtained from the OMNI dataset were used to compute Ey and assess its correlation with IMF-Bz through statistical and scatter-plot analyses. Time-series plots of Dst, IMF-Bz, solar-wind speed, density, and Ey were constructed to identify the coupling between solar-wind drivers and geomagnetic activity. The results demonstrate that strong southward IMF-Bz enhances Ey, which in turn intensifies geomagnetic disturbances indicated by Dst reductions. Corresponding TEC enhancements and depletions reveal significant restructuring of the ionosphere during storm main and recovery phases. This integrated approach provides improved understanding of solar-wind–magnetosphere–ionosphere coupling and the dynamic behavior of ionospheric TEC under varying geospace conditions. The enhancements and disturbances in the solar wind field due to combined co-rotating interaction region (CIR) and CH HSS influences likely resulted in isolated periods of G1 storm levels late on 23 March and isolated G4 storm levels on 24 March. The Dst index value showed a sudden commencement with a sudden increase to 24nT and then decreased continuously to -163nT on March 24, 2023, which is the largest storm so far in solar cycle 25. The IMF-Bz developed a prolonged and significant southward component reaching a minimum of about -20 nT at 03:00 UT, which corresponds to the peak of the minimum Dst index of -163 nT. Solar wind pressure shows a jump from 1.83 nPa on March 22, 2023, to 14.79 nPa on March 23, 2023. Rapid increases in solar wind dynamic pressure compress the Earth’s magnetosphere and rapidly restructure the electrodynamics within. The enhancement of TEC towards the southern hemisphere high latitude was observed. On March 24, 2023, an enhanced spatial distribution of TEC coverage is over the globe. These all evidences might be the result of the geomagnetic storms.

Keywords: Geomagnetic storm, CME, Dst index, Solar flare, Solar wind, TEC.

1. INTRODUCTION

A geomagnetic storm is a major disturbance of Earth’s magnetosphere that occurs when there is an exchange of energy from the solar wind into the space environment surrounding Earth. During storms there is a high variation in the solar wind that produces major changes in the

Submitted: 10th December 2024 ***Accepted: 25th December 2025*** ***Published:2nd May 2026***

currents, plasmas, and fields in Earth's magnetosphere and ionosphere regions. The mid- high and low-latitude ionosphere thermosphere system undergoes large disturbances due to electrodynamics, dynamics, and composition variations (Hintsa and Gebregiorgis, 2017). This is even more effective and can generate significant changes in the storm produced ionospheric electron density structures when geomagnetic storm occurs (Aa et al., 2023; Gizaw and Gebregiorgis, 2014). Typically, geomagnetic storms affect large portions of globe after the changes in IMF-Bz, global electric currents and have patterns that can be recognized in the geomagnetic field (Tamara et al., 2016). Although the ionospheric response to the geomagnetic storm is relatively complex, the ionospheric electron density may get enhanced or depleted during geomagnetic storm, which is commonly known as positive or negative ionospheric storms. The cause of geomagnetic storms is variation in the solar wind parameters, that is enhancement in solar wind speed and solar wind particles that increase solar wind pressure, and at least >3 hr sustained IMF_Bz southward on the day side magnetosphere (Rukundo, 2023). Coronal mass ejections (CMEs) are major solar driver of this disturbance embedded with large plasma emissions from the sun, taking several hours or days to reach the Earth's atmosphere. These mass ejections carry a bulk of solar material in the range10^{11} - 10^{13} kg and the huge amount of energy involved in such ejection processes is believed to be stored in the magnetic fields surrounding the mass ejection site. The structure associated with CMEs has a typical spatial size of about 1 radius of the sun at the base of the corona and expands at velocities from a few tens to 2000 km/s (Mujiber et al., 2010). CMEs can lead to intervals of prolonged southward interplanetary magnetic fields in the resulting disturbances or ICMEs. Other sun's emissions like high solar wind speed from coronal holes, and corotating interaction regions also contribute to geomagnetic storms as described by Rukundo (2023) and references therein. However, the Earth's magnetic field shields the Earth and its atmosphere from the solar wind. This magnetic shielding is not perfect. A fraction of the mass, energy, and momentum from the solar wind can transfer to the magnetosphere and ionosphere through processes that are often referred to as solar wind-magnetosphere interactions (Tsurutani et al., 2020). Gonzalez et al. (1999) and references therein pointed out that with Dst < -100 nT the interplanetary dusk ward electric fields (V×B) were greater than 5 mV/m over a period exceeding 3 hours. The electric field condition is approximately equivalent to Bz = -10 nT. In general, as Singh et al. (2010) and references therein pointed out that, the geomagnetic field measured at any point on the earth's surface is a combination of several magnetic fields generated by various sources. Intense geomagnetic storms generally occur when solar wind having intense, long- duration southward interplanetary magnetic fields (IMF) interact with earth's magnetosphere. It has been known that the intensity of geomagnetic storm is proportional to the interplanetary dawn-dusk electric field E = −V sw × Bz, where Vsw is the solar wind flow speed and Bz is the southward component of the IMF. Different authors like Gopalswamy (2009) have established that if a CME originates close to the disk center and arrives at Earth with a southward magnetic field component, it will cause a geomagnetic storm and coronal mass ejections (CMEs) are the major cause for large geomagnetic storms. High- speed streams (HSS) in corotating interaction regions (CIRS) cause only moderate to weak storms (−100nT < Dst < −50nT). The earth's main field varies slowly in time and creates a cavity in interplanetary space called the geomagnetosphere, where the earth's magnetic field dominates the magnetic field of the solar wind (Astafyeva et al., 2018).

2. DATA AND METHODS

2.1. Data Source

For our study, hourly resolution OMNI-web data, was obtained from the OMNI-web data explorer, the data are available on the OMNIWeb database (https://omniweb.gsfc .nasa.gov/form/dx1.html). Geomagnetic storms can be categorized, in terms of geomagnetic activity index (Dst), into four categories: super storm < −250 nT major (intense or great) storms, 100 nT < Dst < −250 nT, moderate storms falls −50 and −100 nT; and weak storms, −30nT < Dst < −50 nT. While CMEs observed from coronagraphs along the Sun Earth line which are the most geoeffective CME type are taken from website the SOHO/LASCO CME catalogue (http://cdaw.gsfc.nasa.gov/CME_list/halo/ halo.html). While the Dst data is provided by the World Data Center for Geomagnetism, Kyoto (http://swdcdb. kugi.kyoto-u.ac.jp/). While, the global TEC map is obtained from https://stdb2.isee.nagoya-u.ac.jp/GPS/ shinbori/AGRID2/nc/index.html. TEC measurements were obtained from GNSS-based ionospheric monitoring system Global ionospheric Maps (GIMs) with a temporal resolution of 2 hrs and a spatial grid of typically 2.5^0 x 5^0 (latitude x longitude were used.

2.2. Methodology

All datasets (TEC, IMF_Bz, Ey, solar wind parameters and Dst) were resampled to hourly temporal resolution to enable direct comparison. Time-tag offsets due to propagation delays from spacecraft to the magnetopause were corrected using OMNI data's time-shifted format. Convictive electric fields (Ey) were calculated using Ey= -Vsw x Bz. TEC maps were examined to identify for storm- time study as $\delta TEC = TEC_{storm} - TEC_{quiet}$ Spatial patterns were visualized using color coded global maps. To determine the relationship between the IMF-Bz component and the solar wind electric field Ey the corresponding time series of Bz and Ey were extracted and a scatter plot of Ey vs Bz was constructed to evaluate how IMF orientation controls the dayside reconnection electric fields. Data analysis and visualization were carried out usin MATLAB software.

3. RESULTS AND DISCUSSION

3.1. Event Description

The second severe geomagnetic storm (G4) in Solar Cycle 25, was observed during 23-25 March 2023. The effects were primarily due to coronal whole high-speed stream (CH HSS) effects, although sideway influence from a coronal mass ejection (CME) that left the sun on 20 March is also possible candidate on 23 March. The enhancements and disturbances in the solar wind field due to combined co-rotating interaction region (CIR) and CH HSS influences had likely resulted in isolated periods of G1 storm levels late on 23 March and isolated G4 storm levels on 24 March. Halo CME were erupted from the sun that is left the sun at round 15:48 on March 20, 2023 and its impact on the magnetosphere were observed starting March 23, 2023. Solar wind speeds were more than 600 km/s and with this speed it takes nearly 70 hrs to reach the magnetopause. A CIR has resulted from the interaction of high-speed stream with the relatively slower ambient solar wind speed and forms a compression region ahead of the HSS. The main storm activity was started at around 12:00 UT on 23 and reached its minimum value (-163nT) at 3:00 UT on May 24. The recovery phase took about 45 hrs to its normal state. The severe geomagnetic storm was caused probably by a CME eruption associated with solar flares B, C, and M erupting successively on 20th March from about 14:05 UT to 14:42 UT. The interplanetary shock wave arrived at the Earth's magnetosphere and initiated a storm sudden commencement (SSC) at 8:00 UT on 23rd March 2023 and this can be seen from the Dst index. Figure 1 shows from top to bottom are the Dst index top left panel, IMF-Bz (GSM coordinates) top right panel, the solar wind middle left, proton density middle right, solar wind Temperature bottom left and the y component of dawn-dusk electric field bottom left respectively. This was characterized by magnetospheric, and ring current disturbances marked by an induced impulse of 20.1 nT in the IMF-Bz as shown in figure 1.

The behavior of the southward IMF-Bz played a significant role in the geomagnetic activity. The IMF-Bz shows rapid fluctuation between north and southwards and when turned southward, due to the reconnection with the earth's magnetic field enables solar wind energy to transfer into earth's magnetosphere more effectively and this triggers geomagnetic storm.

After that, IMF-Bz developed a prolonged and significant southward component reaching a minimum value of -20 nT at 03:00 UT which corresponds to the peak of the minimum Dst index at -163 nT. The solar wind pressure shows a jump from 1.83 nPa on March 22, 2023 to 14.79 on March 23, 2023. Rapid increases in solar wind dynamic pressure compress the Earth's magnetosphere and caused rapidly restructured the electrodynamics within. The propagation of pressure pulse effects into the magnetosphere caused geomagnetic storm sudden commencement (SSC) likely is driven by pressure pulses with higher magnitude. The dawn-dusk electric fluctuation fluctuates based on the influence of the interplanetary magnetic field fluctuation has shown flipping between east and west.

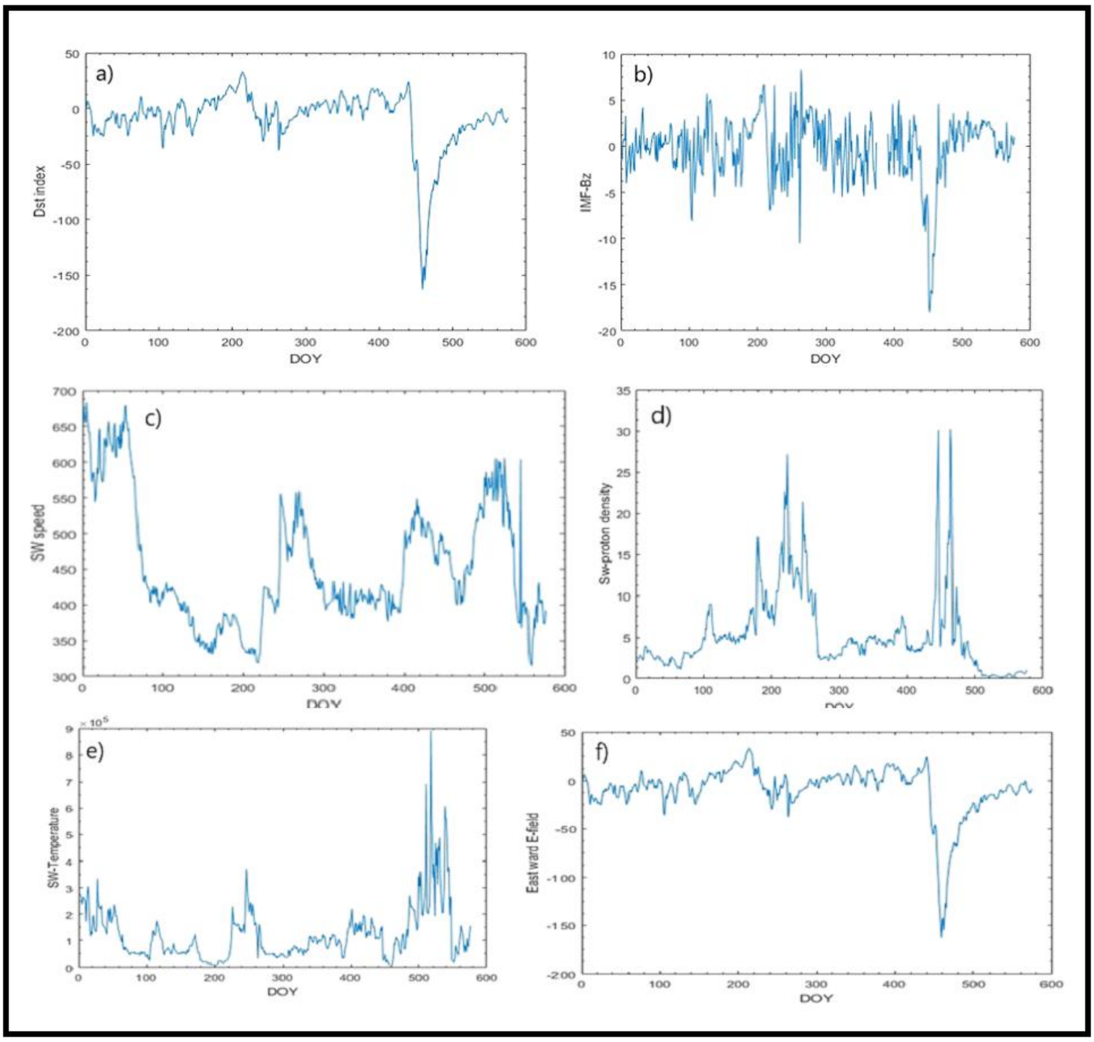

Figure 1. Dst index top left panel, IMF-Bz top right panel, solar wind speed middle left panel, proton density middle right panel, Temperature bottom left panel, and East ward electric field bottom right panel.

3.2. Response of Global Ionospheric TEC to the Geomagnetic Storm

To examine TEC variations, we evaluated global TEC maps at 3:00 Universal time (UT) during the quiet time (pre-storm phase), main phase, and recovery phase of the 2023 March storm. Figure 2 shows TEC Variation from March 21 to March 25, 2023. During pre-storm times the global TEC spatial distribution at 3:00 UT shows higher in the Asian sector as it is local noon at these areas. Maximum TEC is also localized in the mid and South American sectors. However, during the storm time, the enhancement of TEC towards the southern hemisphere high latitude was observed. On March 24/ 2023, enhanced spatial distribution of TEC coverage is over the globe is increased.

Variations of δTEC could be attributed to source of information on the changes in the ionosphere. According to these data, the bursts of δTEC occurred at the beginning of the magnetic disturbance. The duration of these bursts varied within several hours. The behavior of δTEC along American sector, pre- storm time and post storm time showed enhancement in latitude from 30^0 N to -30^0 S at a time of 3:00 UT. However, during the disturbed days, at thesame time the enhancement is observed in latitude from 30^0 N to -60^0 S.

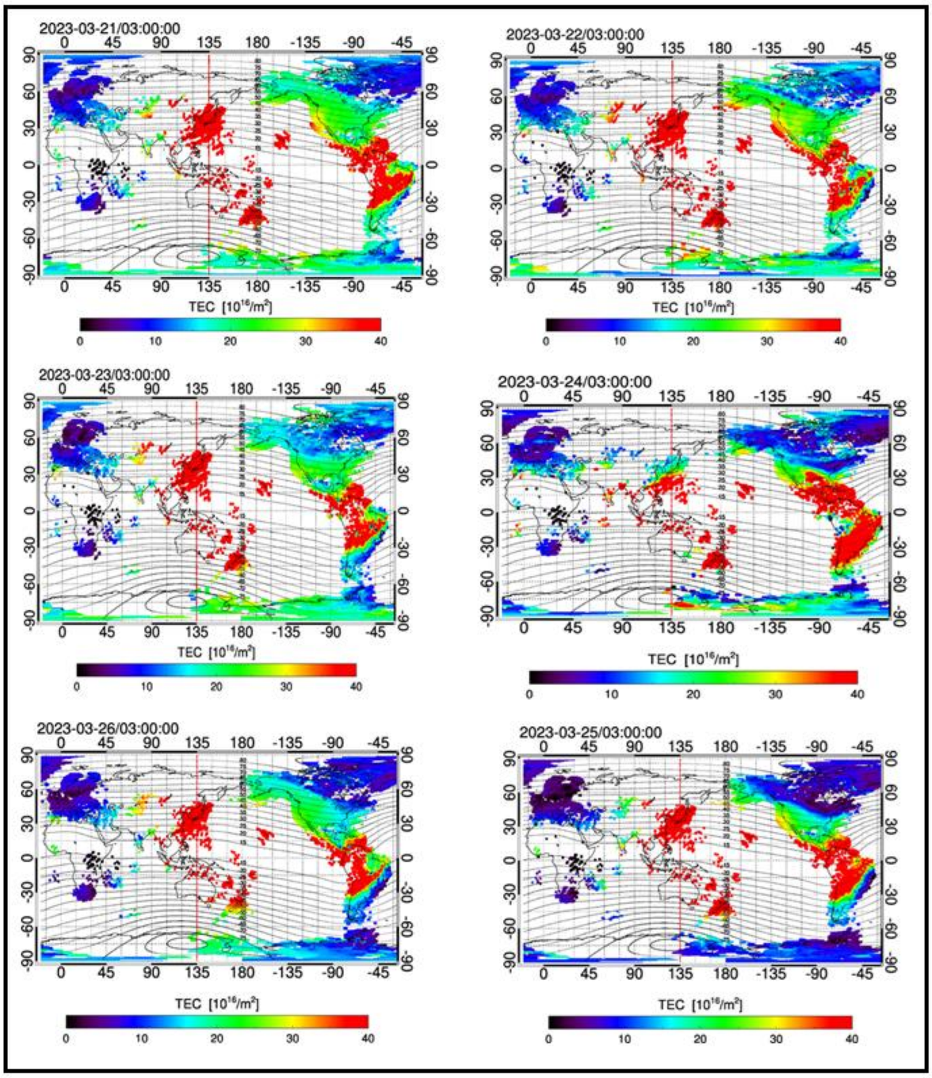

Figure 2. TEC distribution pre storm March 21 and 22, during March 23 and 24, after geomagnetic storm of March 25-26 /2023.

3.3. Correlation between IMF_Bz and Eastward Electric Field (Ey)

Analyzing the IMF-Bz and Ey correlation, particularly with time lagged effects, provides insight into the solar wind- magnetosphere coupling mechanisms that drive geomagnetic storms. Figure 3 shows strong correlation left panel between the IMF- Bz and Eastward electric field (Ey) and right panel IMF- Bz versus Dst index. A linear regression model using the IMF-Bz as the independent variable and Ey as the dependent variable, the IMF-Bz becomes more negative to indicate a positive relationship. During the main phase of the storm IMF-Bz and Ey are strongly correlated. When IMF-Bz reached its most negative value, Ey has spiked accordingly due to enhanced ionospheric convection. Similarly, the Dst index also shows a strong negative deviation as the IMF-Bz turns southward. This directly correlates with increased eastward electric field in the ionosphere.

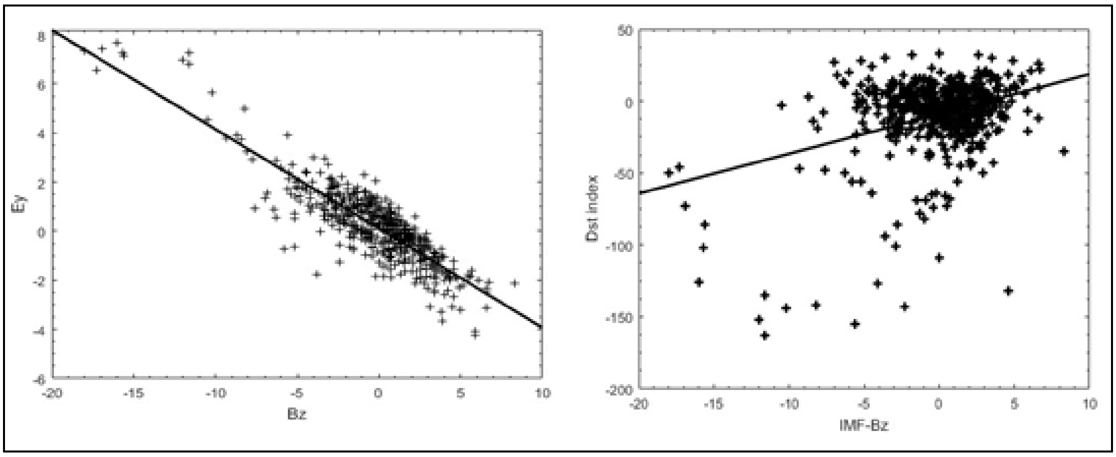

Figure 3. correlation of IMF-Bz vs dawn-dusk electric field left panel and IMF-Bz vs Dst index right panel.

This statistical analysis, especially with cross correlation, can highlight the timing and extent of this relationship, crucial for understanding storm dynamics and improving geomagnetic storm forecasting. Similarly, the Dst index also shows a strong negative deviation as the IMF-Bz turns southward. This directly correlates with increased eastward electric field in the ionosphere.

4. CONCLUSIONS

This study examined the coupled behavior of the solar wind, magnetosphere, and ionosphere by analyzing TEC distributions, the relationship between IMF Bz and the convective electric field Ey, and the temporal evolution of geomagnetic and solar-wind parameters. The results show that periods of strong southward IMF- Bz produce significant increases in Ey, indicating enhanced dayside reconnection and efficient solar-wind energy transfer into the magnetosphere. These intervals coincide with pronounced decreases in the Dst index, confirming the development and intensification of geomagnetic storm phases.

TEC analyses further reveal that the ionosphere responds dynamically to these external drivers. During storm main phases, large-scale TEC enhancements and depletions particularly around low-latitude and equatorial regions highlight the redistribution of plasma driven by thermospheric winds, electric fields, and magnetospheric dynamics. The observed TEC variations closely follow changes in solar-wind and IMF conditions, demonstrating the strong coupling between high-latitude energy input and global ionospheric structure.

Overall, the combined analysis of TEC, IMF Bz, Ey, and geomagnetic indices provides a comprehensive understanding of how solar-wind disturbances propagate through geospace and impact ionospheric electron density. These findings underscore the importance of continuous monitoring of solar-wind parameters to better characterize ionospheric behavior during disturbed conditions and to support applications such as GNSS-based navigation, communication, and space-weather forecasting.

5. ACKNOWLEDGMENTS

The authors express their gratitude to the services NOAA's National Centers for Environmental Information for the opportunity to use OMNIWEB data. Dst indices and global TEC data were obtained from the Data Analysis Center for Geomagnetism and Space Magnetism, Kyoto University, Japan. The authors would like to thank the anonymous reviewers for their contributing comments.

6. CONFLICT OF INTEREST

There is no conflict of interest.

6. REFERENCE

Aa, E., Zhang, S.-R., Erickson, P. J., Wang, W., Qian, L., Cai, X., Coster, A. J & Goncharenko, L. P. 2023. Significant mid- and low-latitude ionospheric disturbances characterized by dynamic EIA, EPBs, and SED variations during the 13–14 March 2022 geomagnetic storm. *Journal of Geophysical Research: Space Physics*, **128**: e2023JA031375, https://doi.org/10.1029/2023JA031375.

Astafyeva, E., Yasyukevich, Y., Maletckii, V., Oinats, B., Vesnin, A & Yasyukevich, A., A. S. 2022. Ionospheric disturbances and irregularities during the 25-26 August 2018 geomagnetic storm. Journal of Geophysical Research: Space Physics, 127, e2021JA029843, https://doi.org/10.1029/2021JA029843.

Gizaw, M. T & Gebregiorgis, A. 2014. Moderate Geomagnetic storms of January 22-25, 2012 and their influences on the wave components in ionosphere and upper stratosphere-mesosphere regions. *Advances in Space Research*, **54(2014)**: 1793–1812.

Gonzalez, W. D., Tsurutani, B. T & Clúa de Gonzalez, A. L. 1999. Interplanetary origin of geomagnetic storms. *Space Science Reviews,* **88**: 529–562, https://doi.org/10.1023/A:1005160129098.

Gopalswamy, N. 2009. Halo coronal mass ejections and geomagnetic storms. *Earth Planets Space,* **61**: 595-597.

Gulyaeva, T. L. 2023. Disturbances in the Magnetosphere and Ionosphere during Spotless Sun. Geomagn. Aeron. 63, 300-308, https://doi.org/10.1134/S0016793222600813.

Hintsa, G. & Gebregiorgis, A. 2017. Global Variations of Ionospheric Total Electron Content (TEC) Derived from GPS Global Ionospheric Maps, (ISSN 2220-184X), **9(2)**: 141-161.

Mujiber, A., Rahman, Manoharan P. K & Umapathy S. 2010, Propagation characteristics of coronal mass ejections and their effects at the near-Earth environment, *J. Radio and Space Physics*, **39**: 276-279.

Rukundo, W. 2023. The ionospheric dynamics of the African sector responding to a severe geomagnetic storm; the storm of 3-5 November 2021. *Space Weather*, **21**: e2022SW003219, https://doi.org/10.1029/2022SW003219.

Singh K., Roopali T & Mishra A. P, 2010. Solar and interplanetary disturbances responsible for geomagnetic storms, *Journal of Physics: Conference Series,* **208**: 012068, https://doi.org/10.1088/1742-6596/208/1/012068.

Tamara, G & Feza, A. 2016. Statistical discrimination of global post-seismic ionosphere effects under geomagnetic quiet and storm conditions. *Geomatics, Natural Hazards and Risk*, **8(2)**: 509-524, https://doi.org/10.1080/19475705.2016.1246483.

Tsurutani, B. T., Lakhina, G. S & Hajra, R. 2020. The physics of space weather/solar-terrestrial physics (STP): what we know now and what the current and future challenges are. *Nonlinear Processes in Geophysics*, **27(1)**: 75-119, https://doi.org/10.5194/npg-27-75- 2020.